MATEC Web of Conferences **14**, 13005 (2014)
DOI: 10.1051/matecconf/20141413005

Dissolution kinetics and morphological changes of γ' in AD730^{TM} superalloy

F. Masoumi[1,a], M. Jahazi[1], J. Cormier[2], and D. Shahriari[1]

[1] Department of Mechanical Engineering, École de technologie supérieure (ETS), H3C 1K3, Montreal, QC, Canada
[2] Institute Pprime, UPR CNRS 3346, Physics and Mechanics of Materials Department, ISAE- ENSMA, 86961 Chasseneuil Cedex, France

Abstract. Alloy AD730^{TM} is a recently developed Nickel base superalloy for application as turbine disk in modern gas turbines with improved thermal efficiency. Ingot casting followed by open die-forging and then heat treatments are the main manufacturing steps for the production of parts made of this alloy. Solution heat treatment operations are applied at different stages of the manufacturing in order to ease the deformation processing and/or prepare the microstructure for final heat treatment. In this research, the influence of various solution heat treatment schedules on morphology and distribution of the γ' phase are investigated and documented. The obtained results will contribute to a better understanding of microstructure evolution of AD730^{TM} during solution heat treatments. Differential Thermal Analysis (DTA) is used for the purposes of measurement of temperatures of phase transformations of the alloy. Based on DTA results, three solutionizing temperatures and three holding times were selected for performing and assessing the solution heat treatment process. Optical and electron microscopy were used to study the morphological evolution as well as the coarsening and dissolution of secondary phases at solvus and subsolvus temperatures. The results indicated that precipitate agglomeration and Ostwald ripening are the governing mechanisms during the initial stages and splitting and partial dissolution of γ' precipitates takes place during subsolvus solution treatments.

1. Introduction

The Ni-based superalloy AD730^{TM}, is a newly developed alloy with superior service properties at 700 °C which will be used for turbine disk applications [1]; however, many of its properties for advanced manufacturing applications are not known. Ni-based superalloys owe their good mechanical strength at high temperatures the precipitation of the $L1_2$ ordered coherent γ' phase in a disordered γ matrix. The γ' characteristics including particle size, morphology, distribution, and volume fraction play important roles in strengthening these alloys [2,3]. Understanding the influence of time and temperature on the γ' phase (Ni_3(Al,Ti)) evolution is of prime importance due to the technological application of superalloys at high temperatures [4]. It is desirable to know the γ' solvus temperature to obtain the optimal material properties during hot deformation processes such as rolling, forging and friction welding. For instance, hot forging of Nimonic alloys is generally performed above the solution temperature of the γ' phase due to significant reduction in flow stress and increase in ductility. It is often observed that the dissolution temperature of the γ' phase does not occur at a single temperature but instead occurs over a range of temperatures, since the as-hot worked microstructure contains inhomogeneous distribution of particle sizes and shapes resulting from, e.g., dendritic segregations [5,6].

The study of microstructural changes for different solution and precipitation treatments in various nickel-based superalloys had been the subject of several research works. For instance, the kinetics of γ' coarsening during aging in Udimet 720 and dissolution behaviour for Nimonic 115 and MAR-M247 superalloys were studied by Monajati et al. [7], Shahriari et al. [8] and Baldan et al. [9], respectively. Grosdidier et.al. [10] showed that dissolution and precipitation process are influenced by the local elastic distortions due to lattice mismatch between γ' and γ phases. Raman et al. [11] have reported Precipitate Agglomeration Mechanism (PAM) as the growth mechanism of particles in the microstructure of IN738LC superalloy. However, no data is available about γ' evolution during solution heat treatments for AD730^{TM}.

In the present study, the effects of heat treatment with the microstructural features of AD730^{TM} are studied to determine the range of γ' dissolution temperature. It is aimed to comprise and compare the two methods of differential thermal analysis (DTA), and conventional heat treatment by metallography evaluation in this article. As the control of volume fraction, size, and morphology of γ' precipitates enhance the performance of this alloy, distribution and morphology of these precipitates are also investigated. Hence, the influence of various solution heat

[a] Corresponding author: Fatemeh.Masoumi.1@ens.etsmtl.ca

Table 1. Chemical composition of AD730^{TM} (wt%) [1].

Ni	Fe	Co	Cr	Mo	W	Al	Ti	Nb
Base	4	8.5	15.7	3.1	2.7	2.25	3.4	1.1

treatments on microstructural evolution of AD730^{TM} is considered. Specifically, the dissolution behaviour of γ' under different experimental conditions is determined and the operating mechanisms are discussed.

2. Experimental procedures

2.1. Material

The chemical composition of AD730^{TM} material used in this study is given in Table 1. Specimens with dimensions of $5 \times 5 \times 5\,mm^3$ were used as samples for heat treatments.

2.2. Thermal analysis

The DTA was carried out using Diamond TG/DTA PerkinElmer with Pt crucible and flowing air atmosphere. The DTA samples ($2 \times 2 \times 0.5\,mm^3$) were heated at a rate of 120 °C/min up to 1180 °C and cooled down to the room temperature by the same rate. Samples for heat treatment trials were prepared by cutting small pieces from the material. Holes of 2 mm in diameter were drilled in the center of one face to a depth of 2 mm for insertion of a thermocouple. All tests were conducted on the samples with the thermocouples attached. In order to study the effect of solution temperature on γ' dissolution, three treatment cycles at 1080 °C, 1100 °C, 1110 °C were selected. The specimen were held for three different times (1.5-min, 30-min, 60-min) at the corresponding temperature and then quenched in iced salt water by a rate of 300 °C/s. For each test the heating and cooling profile were recorded by a computer- aided electronic device using attached thermocouple to the specimen.

2.3. Metallography

For microstructure studies, the samples were mounted and polished using standard metallographic techniques. After etching, the specimens' microstructures were studied by optical and scanning electron microscopy (SEM). The effects of high temperature exposures for long as well as short durations on initial microstructure were studied. Characterization of the size and morphology of the precipitate particles was conducted at micro scales using Hitachi SU70 SEM in secondary electron (SE) mode. The back-scattered electrons (BSE) images are recorded from polished cross sections by use of a backscattered electron detector attached to SEM. In addition, distribution mapping of the different chemical elements constituting the specimen obtained by Energy Dispersion Spectrometer (EDS) in back-scattered electrons (BSE) mode. Analyses were carried out at the microscopic scale using small and high magnification SEM images such as 2000x, 50000x and 100000x to investigate γ' morphology. The average dimensions and volume fraction of the γ' precipitates were quantified using digitized images and standard image analysis software.

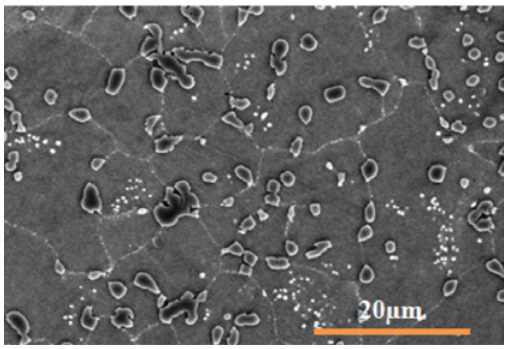

Figure 1. SEM microstructure of the as-received AD730^{TM} alloy showing primary and secondary γ'.

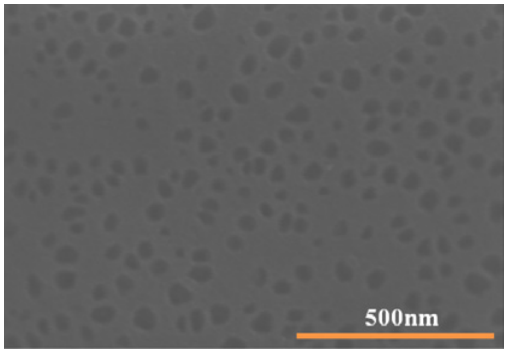

Figure 2. SEM microstructure of the as-received AD730^{TM} alloy showing tertiary γ'.

3. Results and discussions

3.1. As-received material characterization

The as-received materials were as-forged, heat treated at 1080 °C for 4 hours and then air cooled. The microstructure of AD730^{TM} consists of Ni-based austenitic matrix γ, primary γ' precipitates most of them present at the grain boundaries, secondary and tertiary γ' and two types of carbides (see Figs. 1 and 2). The average size of the primary, secondary and tertiary γ' were determined to be 1.4 μm, 400 nm and 30 nm, respectively. Primary γ' precipitates are oval and have irregular shapes and secondary and tertiary ones are either spherical or cuboidal. The carbides (MC) formed during solidification usually exhibit coarse, random, and globular or blocky and script morphology located inside the γ matrix as well as at the grain boundaries. The second type of carbides is $M_{23}C_6$ which precipitate as films, globules, platelets, lamellae, cells, and usually form at grain boundaries [12,13]. They are smaller than MC types and very close to each other so that their possible merging at high temperature substantially reduces the creep life and ductility. On the other hand, as the morphology of the $M_{23}C_6$ after the second heat treatment cycle is globular and they are located along the grain boundaries, thus, less harmful effects on the hot workability are expected [6,13]. These two types of carbides are shown in Fig. 3. The X-ray mapping results (see Fig. 4) shows that MC carbide particles mainly consist of TiC and NbC whilst the $M_{23}C_6$ particles contain significant amounts of (Cr, Mo, W) (see Fig. 5). The average grain size of as-received AD730^{TM} was

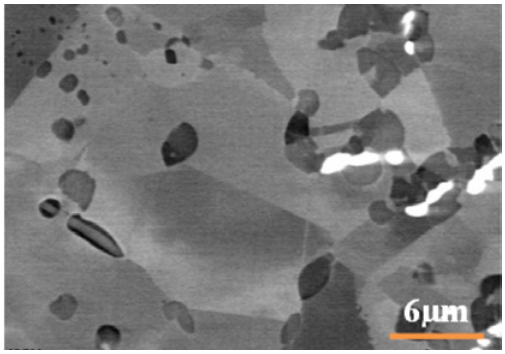

Figure 3. BSE micrograph of carbides in AD730™.

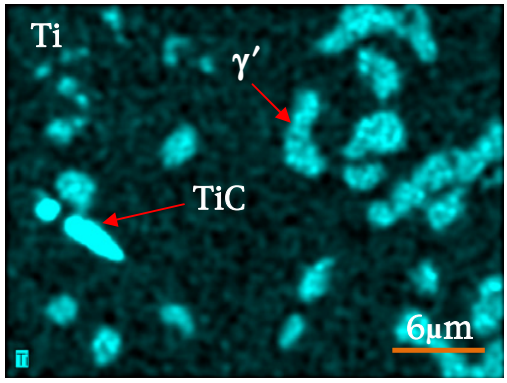

Figure 4. BSE/EDS X-ray maps of the MC carbides indicating they mainly consist of Ti-.

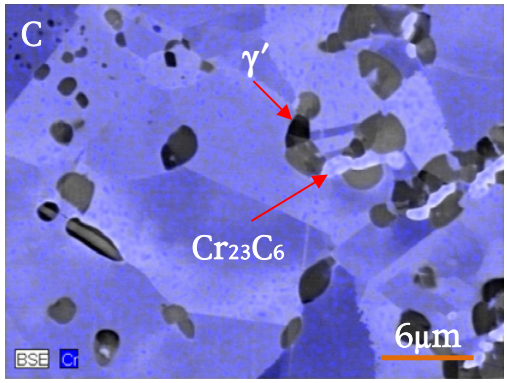

Figure 5. BSE/EDS X-ray maps of the MC carbides indicating they mainly consist of Cr-.

determined according ASTM E112, E930, and E1181 test methods. The average size of the smallest grains is 3 μm, and that of the largest grains is 19 μm. After applying three solution treatments, several microstructural changes were observed. Two different modes of coarsening, precipitate Ostwald ripening and agglomeration, were seen during the initial stages of solution treatments. γ' particles were splitted or dissolved after reaching a critical size (~2–3 μm).

3.2. DTA analyses

Figure 6 shows the differential thermal analysis (DTA) data obtained during heating and cooling cycles with various endothermic and exothermic peaks. The DTA

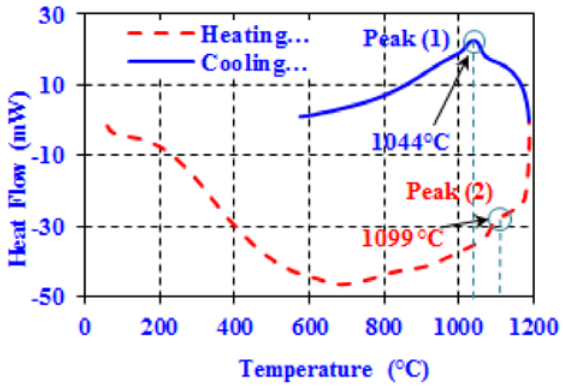

Figure 6. DTA curves showing the various reactions that occur upon (C) cooling and (H) heating of AD730™.

Table 2. Average precipitate size data in AD730™ samples solutionized for various times at three different temperatures.

solutionizing time (min)	1.5	30	60
Temp (°C)	Average particle size (μm)		
1080	1.311	1.334	1.545
1100	1.442	1.579	1.359
1110	1.387	1.085	1.021

peaks are matched to their specific reactions knowing the phases present in the microstructure and the approximate temperatures at which they form [14]. They here correspond to the solvus temperatures of γ'. Two peaks of interest are highlighted in Fig. 6. The small initial peak (1) at approximately 1044 °C in cooling and peak (2) at 1099 °C in heating correspond to the precipitation and dissolution of γ', respectively.

3.3. Effects of heat treatment cycles on dissolution kinetics of γ'

Solution heat treatments were carried out at three different temperatures (1080 °C, 1100 °C, 1110 °C) with three holding times (1.5-min, 30-min, 60-min), to determine the temperature for complete dissolution of γ' and to investigate the morphological evolution of γ' precipitates during various solution treatments. During cooling, the rapid quenching by iced salt water prevented any substantial phase growth which allows comparison of microstructures immediately after treatments.

The average precipitate sizes measured from the resultant microstructures, are given in Table 2. The results show solutionizing at 1080 °C, 1100 °C, and 1110 °C for various time intervals led to gradual precipitate coarsening and dissolving. As a result of the exposure of the alloy to high temperatures for extended periods of time, coarsening, coalescence, and agglomeration of the primary γ' precipitate clearly increased at the expense of the small particles known as secondary and tertiary γ' (see Figs. 7–9). Two different γ' precipitate growth processes were observed: merging of secondary precipitates to produce larger ones that is, both the secondary and primary precipitate particles coarsen with temperature and time by the particle agglomeration mechanism (PAM), and coarsen through solute absorption from the matrix

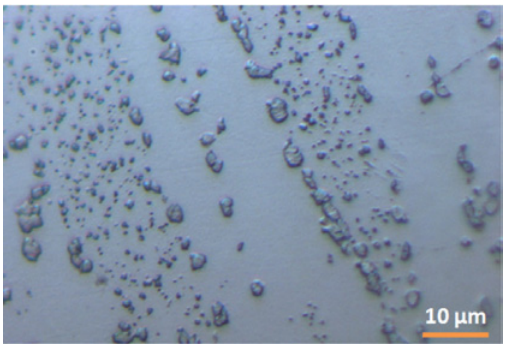

Figure 7. Ostwald ripening as a coarsening mechanism for sample heat treated at 1080 °C for 4 h and air quenched.

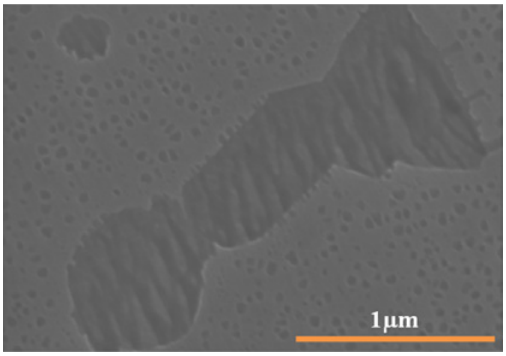

Figure 8. Agglomeration as a coarsening mechanism for sample heat treated at 1080 °C for 4 h and air quenched.

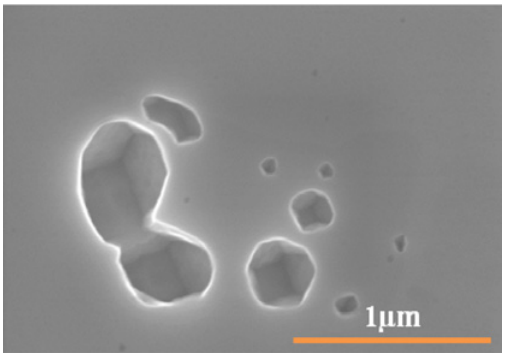

Figure 9. Figure showing necking for agglomeration of particles for sample heat treated at 1080 °C for 4 h and air quenched then solution heat treated at 1100 °C for 1.5 min and water quenched.

(Ostwald Ripening) (see Figs. 7–9). During long periods of solutionizing, coarsening of large precipitates is known to be at the expense of small ones, by the diffusion flux from the small to the large particles, leading to coarsening. Fig. 7 and Fig. 8 also show denuded zones from the fine particles around primary γ' during these heat treatments. In addition, Fig. 1 clearly shows selective coarsening of the precipitate along the grain boundaries, particle agglomeration. Nucleation and growth of precipitates along the grain boundary is known to occur. It can be expected that the precipitates that nucleate on dislocations and grain boundaries grow faster than the precipitates within the grains due to enhanced diffusion of solute atoms in those regions. From the coarsening of precipitates on high angle γ grain boundaries, it can be deduced that there is enhanced solute atom diffusion flux along the particle/matrix interface as soon as two particles are agglomerated. Raman and Balikci [11] reported that PAM rather than Ostwald-ripening mechanism operated in the γ' coarsening process. However, both coarsening mechanisms have been observed in this study. Furthermore, Raman [11] indicate smaller particles migrate as a whole to the nearby coarse particles and join with them, or coalesce with nearby fine ones as well, at relatively high temperatures. This points to the fact that the matrix is considerably softened to enable such migration. However, the occurrence of necking through interaction of diffusion fields between two particles is probably the mechanism of agglomeration in this research rather than migration of the entire particle. Figure 7 and Fig. 8 show, there are denuded zones from the fine particles around primary and secondary γ' during subsolvus heat treatments (1080 °C and 1100 °C). Simultaneously, it appears that tertiary γ' merge to the primary ones periphery (see Fig. 8). In addition, agglomeration takes place between primary particles (see Fig. 8). Since these precipitated particles are close enough to each other, they coalesce forming one particle. Essentially the process involves the overlapping of diffusion fields of the precipitated particles, but not necessarily physical contact in the initial stages. Once the particles have coalesced, the resulting particle shape is then considered to change rapidly to the equilibrium shape by particle/matrix surface diffusion. When the particles touch each other, the coalescence of particles takes place by migration of the interface between them towards the smaller particle. This may be due to the rapid diffusion along the particle/matrix interface as soon as a neck is formed between the two particles. So, agglomeration or coalescence of precipitates creates fewer large particles. Figure 8 and Fig. 9 show neck formation between two adjacent γ' precipitates. Moreover, splitting and partial dissolution of γ' precipitates appears to take place during solution treatment. Initially, when the γ' phase nucleates, it attains spherical morphology to minimize the interfacial energy (dependent on surface area) since the contribution due to strain energy resulting from lattice misfit is low (dependent on volume). With the increasing heating time and temperature, the shape of γ' precipitates changes from spherical to cuboidal to array of cubes [17]. During growth, the contribution of strain energy increases and the precipitates attain cuboidal morphology. However, further growth will increase the strain energy and splitting occurs in order to reduce the strain energy. This is because the decrease in strain energy is larger than the increase in interfacial energy. Doi and coworkers [15] proposed a theoretical model which agreed with the experimental investigations that the effect of strain resulting from lattice misfit can cause splitting of γ' precipitates into eight cuboids. The model also suggested that above a certain lattice misfit magnitude, the precipitates can split to form parallel platelets. γ' splitting phenomenon was also investigated by Hazotte [16] using finite element modelling and showed that the splitting of coherent γ' precipitates occurs due to the effect of strain energy. As Fig. 10 shows, in 1110 °C heat treatments, the primary γ' particles tend to break into smaller ones

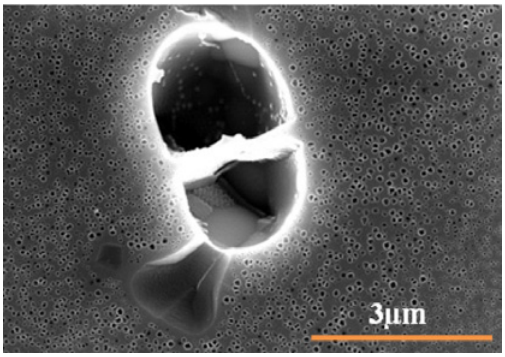

Figure 10. Figure showing splitting of coarse particles into two fragments for sample heat treated at 1080 °C for 4 h and air quenched then solution heat treated at 1110 °C for 30 min and water quenched.

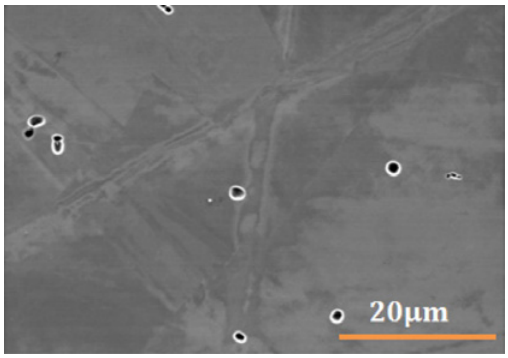

Figure 11. Figure showing dissolution for sample heat treated at 1080 °C for 4 h and air quenched then solution heat treated at 1110 °C for 60 min and water quenched.

and/or dissolve. Only dissolving and splitting was observed at this temperature and coarsening was not observed. Figure 11 shows the minimum primary particle size of γ' (900 nm) and its volume fractions (0.3%) obtained for solution heat treatments at 1110 °C for 60 minute. Thus, it indicates that the extent of dissolution increases as a function of holding temperature and holding time.

3.4. Suppressed γ' nucleation

The solution heat treatment at 1110 °C for 60 minute resulted in almost complete dissolution of primary γ' phase particles and caused very fine unimodal spherical γ' particles to re-precipitate during cooling. Figure 12 shows a large number of extremely fine γ' particles reprecipitated during subsequent cooling process. The size of the reprecipitated γ' is very fine, from a few nm to up to ~20 nm. The fine γ' reprecipitated under fast cooling is spherical in shape. The number density of reprecipitated fine γ' after solution heat treatment and quenching is very high. The spherical shape of the fine reprecipitated γ' results from the small interfacial energy and elastic strain. The former was proportional to the γ/γ' interface area and the latter proportional to the volume of γ' particles. The elastic strain was determined mainly by the lattice mismatch between γ and γ' [17]. In view of the size, shape and distribution of the reprecipitated γ' particles, the value

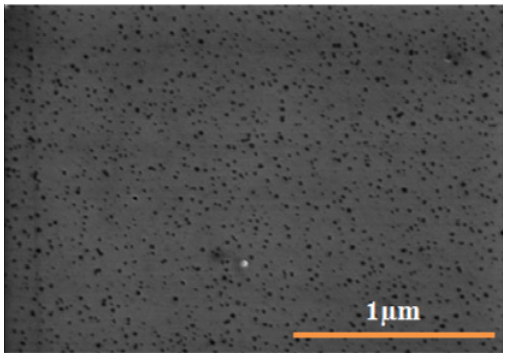

Figure 12. Figure showing dissolution and reprecipitation for sample heat treated at 1080 °C for 4 h and air quenched then solution heat treated at 1110 °C for 60 min and water quenched.

of the lattice mismatch between the reprecipitated γ and γ' matrix in the heat treated material is expected to be smaller than that between parent γ' and γ matrix in the as-received material. In order to determine the critical cooling rate for suppressing γ' precipitation from a supersaturated solid solution, the following analysis is used. Equation (1) helps in predicting the cooling rate of rapidly quenched specimens [18]:

$$-dT/dt = H(T - T_0)/\xi\rho C \tag{1}$$

where ξ, ρ, C, H, T, and T_0 are thickness of the specimen, density, specific heat, heat transfer coefficient, solidification point, and ambient temperature, respectively. They can be calculated from the following equations for AD730^{TM} [19].

$$\rho_{ideal298} = M/V_{ideal} \tag{2}$$

$$M = \sum Xi\,Mi \quad V_{ideal} = \sum 10^6\, V_{ideal298}\,(\mathrm{m}^3/\mathrm{mol}) \tag{3}$$

$$C_{ideal298}\,(\mathrm{J/K/Kg}) = \sum C_{ideal298}\,(\mathrm{J/K/mol})/\mathrm{M} \tag{4}$$

$$\begin{aligned} T_{sol}(K) = {} & -120 + 17.7 \cdot Y_{Ni} + 16.0 \cdot Y_{Co} + 15.2 \cdot Y_{Al} \\ & + 2.1 \cdot Y_{Ti} + 13.4 \cdot Y_{Ta} + 19.2 \cdot Y_{Cr} \\ & + 5.0 \cdot Y_{Mo} + 20.4 \cdot Y_{W} + 34.3 \cdot Y_{Re} \\ & + 23.1 \cdot Y_{Ru} + 15.4 \cdot Y_{Fe} + 6.4 \cdot (Y_{Nb} + Y_{Hf}). \end{aligned} \tag{5}$$

Where $Y_i = 100X_i$ and M is molecular weight and X_i is mole fraction.

From Eq. (1), the minimum cooling rate necessary for suppressing γ' precipitation in AD730^{TM} was estimated to be 5.95×10^4 °K/s. In Fig. 5, a uniform distribution of ultrafine γ is observed. They are nucleated during the final cooling step and cannot grow significantly due to the rapid quenching. This experiment suggests that rapid quenching faster than 5.95×10^4 °K/s can suppress the γ' precipitation. According to the calculated value for cooling rate, reaching this rate in real practical conditions is impossible. So, generally γ' reprecipitation should be observed for AD730^{TM} alloy.

4. Conclusions

1- The equilibrium dissolution temperature of the γ' particles is approximately 1100 °C which is validated by DTA. By conventional heat treatments via microstructure observations, the dissolution temperature is around 1110 °C for about 60 minute. However, after this solution heat treatment still 0.3% primary γ' was observed due to some residual chemical heterogeneity within the alloy.

2- Two types of carbides, MC and $M_{23}C_6$ are observed in AD730™. All MC carbide particles mainly consisting of TiC, NbC and the $M_{23}C_6$ particles contain Cr, Mo, W.

3- The coarsening of primary and secondary γ' precipitates takes place through PAM and Ostwald ripening. Partial dissolution and splitting also occurs simultaneously.

4- Very fine γ' particles with unimodal size distribution are reprecipitated during cooling after solution heat treatments. The mean size of the reprecipitated γ' is smaller than 20 nm. Their shape is spherical and their number density is very high. Quenching faster than 5.95×10^4 °K/s can suppress the γ' reprecipitation for AD730™. As this rate cannot be achieved in industrial applications, γ' reprecipitated will be always observed.

The financial support from the Natural Sciences and Engineering Research Council (NSERC) of Canada in the form of a Discovery Grant is gratefully acknowledged. The authors would like to thank the Aubert & Duval company and especially Dr. Alexandre Devaux for providing AD730™ samples.

References

[1] A. Devaux, B. Picque, M.F. Gervais, E. Georges, T. Poulain, P. Heritier, TMS Superalloys, 911 (2012)

[2] A. Heckl, S. Neumeier, M. Göken, R. F. Singer, Mater. Sci. Eng. A, **528** (9) 3435 (2011)

[3] H. Y. Li, X. P. Song, Y. L. Wang, G. L.. Chen, Rare Met. **29** (2) 204 (2010)

[4] S. Steuer, Z. Hervier, S. Thabart, C. Castaing, T. M. Pollock, J. Cormier, Mat. Sci. Eng. A, **601**, 145 (2014)

[5] N. K. Park, I. S. Kim, Y. S. Na, J. Mater. Proc. Technol. **111**, 98 (2001)

[6] R. J. Siddall, J. W. Eggar, . Mater. Sci. Technol. **2**, 728 (1986)

[7] H. Monajati, M. Jahazi, R. Bahrami and S. Yue, Mater. Sci. Eng. A, **373**, 286 (2004)

[8] D. Shahriari, M. H. Sadeghi, A. Akbarzadeh, M. Cheraghzadeh, Int. J. Adv. Manuf. Technol., **45** (9–10) , 841 (2009)

[9] P. R. S. A. Silva, R. Baldan, C. A. Nunes, G. C. Coelho, A. M. S. Costa, Mater. Charact. **75**, 214 (2013)

[10] T. Grosdidier, A. Hazotte, A. Simon, Mater. Sci. Eng., A **256**, 183 (1998)

[11] I. Roy, E. Balikci, S. Ibekwe, A. Raman, J. Mater. Sci. **40**, 6207 (2005)

[12] S. A. Sajjadi, S. M. Zebarjad, R. I. L. Guthrie, M. Isac, J. Mater. Proc. Technol. **175**, 376 (2006)

[13] J. Safari, S. Nategh, J. Mater. Proc. Technol. **176**, 240 (2006)

[14] G. Hone, W. Hemminger, H.J. Flammersheim, *Differential scanning calorimetry*, (Springer- Verlag, Berlin, 2003)

[15] M. Doi, T. Miyazaki, T. Wakatsuki., Mater. Sci. Eng. **67**, 247 (1984)

[16] A. Hazotte, T. Grosdidier, S. Denis, Scripta Mater. **34**, 601 (1996)

[17] R.C.Reed, *The Superalloys: Fundamentals and Applications.* Cambridge University Press, (2006).

[18] D. Shahriari, M. H. Sadeghi, A. Akbarzadeh, Mater. Manuf. Processes, **24**, 559 (2009)

[19] K. C. Mills, Y. M. Youssef, Z. Li, Y. Su, ISIJ Int. **46** (5) 623 (2006)